PHYSICAL REVIEW D VOLUME 47, NUMBER 9 1 MAY 1993

Tunneling and the spectrum of the Potts model

Jing-Dong Wang and Carleton DeTar

Department of Physics, University of Utah, Salt Lake City, Utah 84112

(Received 24 June 1992)

The three-dimensional, three-state Potts model is studied as a paradigm for high-temperature quantum chromodynamics. In a high-statistics numerical simulation using a Swendson-Wang algorithm, we study cubic lattices of dimension as large as 64^3 and measure correlation functions on long lattices of dimension $20^2 \times 120$ and $30^2 \times 120$. These correlations are controlled by the spectrum of the transfer matrix. This spectrum is studied in the vicinity of the phase transition. The analysis classifies the spectral levels according to an underlying S_3 symmetry. Near the phase transition the spectrum agrees nicely with a simple four-component Hamiltonian model. In the context of this model, we find that low-temperature ordered-ordered interfaces nearly always involve a disordered phase intermediate. We use a spectral method for determining the surface tension between phases.

PACS number(s): 05.50+q, 12.38.Mn, 64.60.Cn

I. INTRODUCTION

The three-dimensional, three-state Potts model has long been studied as a paradigm for the phase structure of quantum chromodynamics (QCD) at high temperature in the heavy quark limit [1]. It has been found that at zero magnetic field, the Potts model has a weak first-order phase transition, separating a low-temperature phase that breaks the $Z(3)$ symmetry and a high-temperature phase in which the symmetry is restored [2]. The underlying $Z(3)$ symmetry requires that at low temperature there be three-ordered or broken symmetry phases with the same free energy. In a finite volume system the behavior of the theory in the vicinity of the phase transition is complicated by tunneling among four phases: the three-ordered phases and the disordered (symmetry-restored) phase.

The Potts model with no magnetic field corresponds to QCD with infinitely heavy quarks—in effect, without any dynamical quarks. In a study of QCD without quarks the APE group found that the correlation length of the system appears to grow as the physical volume is increased, suggesting an infinite correlation length in the infinite volume limit, a characteristic of a continuous phase transition [4]. Doubts were raised that the phase transition is first order. The APE study differed from other contemporary work [5] in measuring correlation lengths on lattices with one long dimension. Two more recent high-statistics studies of the Potts model and of QCD, using different indicators of the order of the phase transition, reconfirmed the first-order character of the phase transition in both models [6, 7]. These more recent studies used a finite-size scaling analysis of susceptibilities to demonstrate a first-order transition. The now widely accepted explanation for the confusion over correlation lengths is that finite volume tunneling among the $Z(3)$-equivalent ordered phases introduces a correlation related to the typical domain size of those phases [3]. This correlation length does indeed become infinite in an infinite volume system, as a natural consequence of the first-order character of the phase transition.

To give an explicit demonstration of the effects of tunneling on correlations and to develop new insight into the thermodynamics of domain boundaries, we have carried out a new study of the three-state, three-dimensional Potts model on lattices with one long dimension [8]. Our study emphasizes the determination of the spectrum of the transfer matrix. We demonstrate explicitly how tunneling modifies the spectrum and, as a consequence, the correlation lengths in the vicinity of the phase transition. Our study parallels work done with the four-dimensional Ising model by Jansen *et al.* [9]. Our work makes it possible to understand the results of the several references [4–7] in a common framework. In the next section we introduce our notation, discuss the S_3 symmetry of the transfer matrix, develop a phenomenological four-component model for tunneling, and introduce the formulas needed for obtaining the spectrum. In Sec. III we present the results of the simulation. We show that the spectrum and interface statistics agree well with predictions of the four-component model. We obtain the surface tension from the spectral splittings. In the final section we state our conclusions.

II. PHENOMENOLOGY OF THE POTTS MODEL

A. Transfer matrix and symmetries

The three-dimensional, three-state Potts model is a classical spin system with one spin s_i on each site $i = (x, y, z)$ of a cubic lattice. Let the lattice dimension be $L_x \times L_y \times L$. Spins take on the values $s_i \in Z(3) = \{1, \exp(\pm 2\pi i/3)\}$. The partition function of the Potts model at zero magnetic field is given by

$$Z(\beta) = \sum_{s_i} \exp\left(-\beta \sum_{(i\mu)} \mathrm{Re}\, s_i^* s_{i+\hat{\mu}}\right), \qquad (1)$$

where $i+\hat{\mu}$ is the nearest-neighbor site in the positive $\hat{\mu}$ direction and the sum s_i is over all configurations of spins. Let the spins on a plane of constant lattice coordinate z be denoted $S_z = \{s_{x,y,z} | x \in 1,\ldots,L_x, y \in 1,\ldots,L_y\}$. Then, as is well known, the partition function can be written as the trace of the transfer matrix raised to the power L:

$$Z(\beta) = \mathrm{Tr}\, T^L, \tag{2}$$

where explicitly

$$\langle S_z|T|S_{z+1}\rangle = \exp\Bigg(-\beta \,\mathrm{Re}\, s^*_{(x,y,z)} s_{(x,y,z+1)} - \beta \sum_{\mu=1,2} \mathrm{Re}\, s^*_{(x,y,z)} s_{(x,y,z)+\hat{\mu}} \Bigg). \tag{3}$$

The expectation value of an operator O on this ensemble is expressed in terms of the transfer matrix as

$$\langle O\rangle = \mathrm{Tr}(T^L O)/\,\mathrm{Tr}\, T^L. \tag{4}$$

The correlation between local operators $A(z)$ and $B(z')$ with $z' > z$ is expressed as

$$\langle A(z)B(z')\rangle = \mathrm{Tr}(T^z A T^{z'-z} B T^{L-z'})/\,\mathrm{Tr}\, T^L. \tag{5}$$

A Hamiltonian matrix H is defined as usual in terms of the transfer matrix so that

$$T = \exp(-H), \tag{6}$$

and the spectral decomposition of the transfer matrix in terms of the eigenvalues E_n of the Hamiltonian H is

$$T = \sum_n |n\rangle \exp(-E_n) \langle n|\,. \tag{7}$$

Let $n = 0$ denote the ground state. The correlation between two local operators A and B is then written in terms of the spectrum as

$$\langle A(z)B(z')\rangle = \frac{\sum_{mn} \langle m|A|n\rangle \langle n|B|m\rangle \exp[-(E_n - E_m)(z'-z)] \exp(-E_m L)}{\sum_m \exp(-E_m)L}. \tag{8}$$

In this way correlations between local operators give information about the spectrum of the transfer matrix. (Of course, only the energy level differences $(E_n - E_0)$ have physical significance.)

The Potts model is symmetric under global transformations of the threefold permutation group S_3. These transformations are generated by

$$s_i \to e^{\pm 2\pi i/3} s_i, \quad s_i \to s_i^* \quad \forall_i. \tag{9}$$

Therefore each of the eigenstates of H and each of the operators of interest O can be classified according to the three irreducible representations S (symmetric), A (antisymmetric), and M (mixed, two dimensional). For example, the spin operator, itself, belongs to M, the operator $|s|^2$ belongs to S, and the operator $\mathrm{Re}\, s_i \,\mathrm{Im}\, s_j - \mathrm{Im}\, s_i \,\mathrm{Re}\, s_j$ belongs to A.

B. Simple model

To begin with the classification of states, consider first the extreme case $\beta \to \infty$. As is well known, the statistical ensemble reduces to three configurations of equal weight, with all spins aligned in either of the three $Z(3)$ directions. In the Hamiltonian language the ground state of H at infinite β is threefold degenerate, with all spins on the (x,y) plane aligned in one of the three directions. Call these three states $|1\rangle$, $|2\rangle$, and $|3\rangle$. These states are related by a $Z(3)$ transformation R as follows:

$$|2\rangle = R|1\rangle, \quad |3\rangle = R|2\rangle. \tag{10}$$

At the other extreme, $\beta = 0$, the statistical ensemble contains all spin configurations with equal weight, and the ground state of the Hamiltonian is not degenerate. Call it $|0\rangle$. These states have finite-β counterparts.

Beginning from these extremes, we introduce a phenomenological model for the spectrum at intermediate β in a finite volume system. As β is decreased from infinity, mixing between the three degenerate states occurs. Because of the S_3 symmetry, the Hamiltonian matrix must be approximately of the form

$$\begin{pmatrix} 0 & \epsilon & \epsilon \\ \epsilon & 0 & \epsilon \\ \epsilon & \epsilon & 0 \end{pmatrix}. \tag{11}$$

As a result of mixing, the degeneracy of the three states is lifted, giving rise to a symmetric ground state $|0s\rangle = |1\rangle + |2\rangle + |3\rangle$ and a twofold degenerate mixed-symmetry state $|0m\rangle$ of slightly higher energy. The mixing parameter ϵ depends on the transverse area $L_x L_y$. Since mixing between the degenerate vacuums requires a rearrangement of the spins over the entire (x,y) plane, it is plausible that the dependence is

$$\epsilon = \exp(-\beta L_x L_y \alpha(\beta)), \tag{12}$$

where $\alpha(\beta)$ is the surface tension for the interface. Indeed at large β it is easily shown that $\alpha(\beta) = 3/2$.

In the infinite volume system a phase transition takes place at $\beta = \beta_c$. In a finite volume, crossover occurs at β_c, where many observables change rapidly. For $\beta < \beta_c$ the ground state $|0s\rangle$ is then identified with the restored-symmetry-phase (disordered) vacuum $|0\rangle$, and the mixed symmetry state $|0m\rangle$ is identified as the lowest-lying mixed-symmetry excitation of the symmetric vacuum.

If the phase transition is first order, all four states coexist. Thus to model the rounding of the phase transition, we write the Hamiltonian on the simplified basis of the

four unmixed vacuum states, $|0\rangle$, $|1\rangle$, $|2\rangle$, and $|3\rangle$ as [15]

$$\begin{pmatrix} \Delta & \lambda & \lambda & \lambda \\ \lambda & 0 & \epsilon & \epsilon \\ \lambda & \epsilon & 0 & \epsilon \\ \lambda & \epsilon & \epsilon & 0 \end{pmatrix}. \tag{13}$$

The row and column labels are in order $0, 1, 2, 3$. The parameter $\Delta = \alpha(\beta - \beta_c)$ with $\alpha > 0$ is the energy difference between the disordered (symmetric) phase state $|0\rangle$ and the degenerate ordered phase (broken symmetry) states $|1\rangle$, $|2\rangle$, $|3\rangle$. This difference vanishes at crossover. The parameter λ gives the mixing strength between the disordered phase vacuum $|0\rangle$ and the degenerate ordered phase vacuums, and the parameter ϵ gives the direct mixing strength between the ordered vacuums. The eigenenergies are

$$\begin{aligned} E_{0s} &= \epsilon + \tfrac{1}{2}\Delta - \tfrac{1}{2}\sqrt{\Delta^2 - 4\epsilon\Delta + 4\epsilon^2 + 12\lambda^2}, \\ E_{0m} &= -\epsilon, \\ E_{1s} &= \epsilon + \tfrac{1}{2}\Delta + \tfrac{1}{2}\sqrt{\Delta^2 - 4\epsilon\Delta + 4\epsilon^2 + 12\lambda^2}. \end{aligned} \tag{14}$$

As expected, there are two states belonging to the symmetric representation of S_3: one, the ground state $|0s\rangle$ and the other, an excited state $|1s\rangle$; and there is one twofold degenerate mixed symmetry state $|0m\rangle$ as before. For large β we expect the state $|1s\rangle$ to become degenerate with a new excited mixed symmetry state $|1m\rangle$ (not included in the four-component model), in the same pattern as the $|0s\rangle$ and $|0m\rangle$ states. With our criteria for assigning transverse planes to the four phases (see Sec. III B below), the numerical simulation indicates that $\epsilon << \lambda$. Thus in the region $\epsilon << |\Delta|$, we may approximate the energy levels with

$$E_{0s} = \tfrac{1}{2}\Delta - \tfrac{1}{2}\sqrt{\Delta^2 + 12\lambda^2}, \tag{15}$$

$$E_{0m} = 0, \tag{16}$$

$$E_{1s} = \tfrac{1}{2}\Delta + \tfrac{1}{2}\sqrt{\Delta^2 + 12\lambda^2}. \tag{17}$$

Figure 1 summarizes the expected behavior of the excitation energies, as a function of $\alpha(\beta - \beta_c)/\lambda$, relative to the ground-state energy, which has been renormalized to zero in this figure. The lowest two energy differences in this figure come from Eqs. (15)–(17) and the energy difference E_{1m} is simply a sketch. We see that in a finite system the crossover results in a smooth connection between the energy levels on either side of β_c. In the infinite volume limit the crossover is much more rapid and the upper wings of the curves in Fig. 1 level off as a consequence of higher-level crossings.

By introducing a four-level system we have assumed a first-order phase transition. In a continuous phase transition the states $|0\rangle$ and $|0s\rangle$ should be equivalent, and a three-level system would suffice. Although the model focuses on the lowest few levels, it can, of course, be enlarged to incorporate other excited levels as well. Indeed, in order to incorporate the excited levels quantitatively, at least eight levels are needed: four for the states already considered, and four more for the corresponding excited states.

Let us be more explicit about the excitations of the

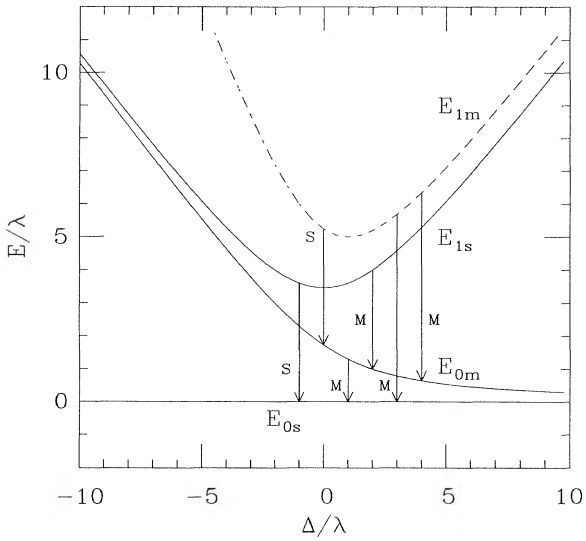

FIG. 1. Phenomenological model of the lowest three energy levels at crossover. The ground-state energy has been adjusted to zero at all β. The level E_{1m} does not come from the model; it is based merely on a guess. The others come from the four-component model equations (15)–(17). Transitions induced by a mixed operator are indicated with "M" and a symmetric operator with "S."

ordered phase. In the infinite volume limit these vacuums are not mixed. We postulate that the lowest excitation of the state $|1\rangle$ is a state $|1*\rangle$ of mixed symmetry, reachable by acting on the vacuum with the zero-momentum spin operator

$$s(z) = \sum_{x,y} s_{(x,y,z)}. \tag{18}$$

We shall often refer to the corresponding Schrödinger-picture operator $s \equiv s(0)$. Without loss of generality we introduce only one new state as

$$s\,|1\rangle = \gamma\,|1\rangle + \delta\,|1*\rangle\,. \tag{19}$$

The corresponding excitations in the other vacuums are reached by a $Z(3)$ transformation R in analogy with Eq. (10) as follows:

$$|2*\rangle = R\,|1*\rangle\,, \quad |3*\rangle = R\,|2*\rangle\,. \tag{20}$$

Since $RsR^{-1} = \exp(-2\pi i/3)s$, the $Z(3)$ symmetry requires

$$s\,|2\rangle = e^{2\pi i/3}(\gamma\,|2\rangle + \delta\,|2*\rangle), \tag{21}$$

$$s\,|3\rangle = e^{-2\pi i/3}(\gamma\,|3\rangle + \delta\,|3*\rangle). \tag{22}$$

Now just as mixing between the degenerate vacuums leads to a symmetric state $|0s\rangle$ and two mixed symmetry states $|0mk\rangle$ ($k = 1, 2$ labels the two degenerate components), we expect mixing among the excited-state counterparts to result in a symmetric state $|1s\rangle$ and a mixed symmetry state $|1mk\rangle$. With this notation we are implicitly identifying these states with the levels of Fig. 1.

From the S_3 symmetry we then obtain explicit formulas for the matrix elements of the spin operator between these states:

$$\begin{aligned}
&\sum_{k=1,2} |\langle 1s|\, s\, |0mk\rangle|^2 = \delta^2, \\
&\sum_{k=1,2} |\langle 0s|\, s\, |0mk\rangle|^2 = \gamma^2, \\
&\sum_{k=1,2} |\langle 0s|\, s\, |1mk\rangle|^2 = \delta^2, \\
&\sum_{k=1,2} |\langle 1s|\, s\, |1mk\rangle|^2 = \gamma^2.
\end{aligned} \tag{23}$$

We note also that if mixing among the degenerate states is weak the symmetric operator $|s|^2$ satisfies

$$\left|\langle 1s|\, |s|^2\, |0s\rangle\right|^2 = \sum_{k=1,2} \left|\langle 1mk|\, |s|^2\, |0mk\rangle\right|^2. \tag{24}$$

C. Correlations

We now write working formulas for the correlations between the spin operators s and $|s|^2$, based on the lowest-lying levels discussed above.

First, we observe that matrix elements must obey selection rules of the S_3 symmetry. For example, the spin operator s is of mixed symmetry. The two components of the operator are just $(\mathrm{Re}\, s, \mathrm{Im}\, s)$. Thus matrix elements $\langle n|\, s\, |m\rangle$ vanish if $|m\rangle$ and $|n\rangle$ are both symmetric. Since $|s|^2$ is a symmetric operator, matrix elements $\langle n|\, |s|^2\, |m\rangle$ vanish if $|m\rangle$ and $|n\rangle$ are not in the same S_3 representation.

Therefore, the leading nonvanishing terms in the correlation for $|s|^2$ from Eq. (8) are

$$\begin{aligned}
\langle |s(z)|^2 |s(0)|^2\rangle = {} & \left|\langle 0s|\, |s|^2\, |0s\rangle\right|^2 + \left|\langle 1s|\, |s|^2\, |0s\rangle\right|^2 [e^{-E_{1s}z} + e^{-E_{1s}(L-z)}] \\
& + \left|\langle 1m|\, |s|^2\, |0m\rangle\right|^2 [e^{-(E_{1m}-E_{0m})z} + e^{-(E_{1m}-E_{0m})(L-z)}] e^{-E_{0m}L},
\end{aligned} \tag{25}$$

and for s it is

$$\begin{aligned}
\langle s(z)s^*(0)\rangle = {} & |\,\langle 0m|\, s\, |0s\rangle\,|^2 [e^{-E_{0m}z} + e^{-E_{0m}(L-z)}] + |\,\langle 1m|\, s\, |0s\rangle\,|^2 [e^{-E_{1m}z} + e^{-E_{1m}(L-z)}] \\
& + |\,\langle 1s|\, s\, |0m\rangle\,|^2 [e^{-(E_{1s}-E_{0m})z} + e^{-(E_{1s}-E_{0m})(L-z)}] e^{-E_{0m}L} \\
& + |\,\langle 1m|\, s\, |0m\rangle\,|^2 [e^{-(E_{1m}-E_{0m})z} + e^{-(E_{1m}-E_{0m})(L-z)}] e^{-E_{0m}L}.
\end{aligned} \tag{26}$$

The six transitions taken into account in these expressions are indicated in Fig. 1.

Clearly, in order for the several transitions for be discernible in the fits to correlation functions, it is necessary that the spectral components be both strong and well separated. With our data we are able to distinguish two spectral components for the mixed operator and find only one significant spectral component for the symmetric operator. These transitions correspond to dropping all terms with the factor $\exp(-E_{0m}L)$. For the mixed operator, this approximation can be justified as follows. (1) Over the range $\beta < \beta_c$, the factor $\exp(-E_{0m}L)$ is small (at the largest, of order 1/10). This factor multiplies the third term on the right-hand side (RHS) in both expressions and the fourth term in the second expression. Appealing to our phenomenological model and Eqs. (23) and (24), which makes it possible to compare the second and third terms, we see that we may drop terms in $\exp(-E_{0m}L)$ from the summation, thereby eliminating all transitions leading to the level E_{0m}. (2) Over the range $\beta > \beta_c$, the spectral lines for all transitions from the levels $1s$ and $1m$ to $0s$ and $0m$ are too close to be resolvable with our statistics. Thus the second spectral component in the mixed operator is presumably a composite of all three transitions permitted by the selection rules. For the symmetric operator our failure to locate the second spectral component presumably reflects an insufficiently strong coupling to this operator.

We are left, finally, with a three-parameter expression for the symmetric operator and a four-parameter expression for the mixed operator:

$$\begin{aligned}
&\langle |s(z)|^2 |s(0)|^2|\rangle = A_1 + A_2[e^{-E_{1s}z} + e^{-E_{1s}(L-z)}], \\
&\langle s(z)s^*(0)\rangle = C_1[e^{-E_{0m}z} + e^{-E_{0m}(L-z)}] + C_2[e^{-E_{1m}z} + e^{-E_{1m}(L-z)}].
\end{aligned} \tag{27}$$

III. NUMERICAL SIMULATION

Since the simulation of tunneling effects requires an algorithm that gives efficient and rapid sampling of the phase space, particularly in the crossover region, we used the Swendson-Wang (SW) algorithm [10]. The code was checked by comparing measured observables in selected extensive runs with results from simulations using a heat bath algorithm.

Simulations were carried out on cubic lattices of size N^3, for $N = 16$, 20, 24, 30, 48, and 64 in order to confirm the first-order nature of the phase transition through the use of finite-size scaling analysis. For this purpose we measured the specific heat and the fourth-order cumulant. Table I summarizes the extent of this data sample. The majority of the simulations were carried out on

TABLE I. Data sample for cubic lattices.

V	β	Sweeps (10^6)
16^3	0.3663	0.6
20^3	0.3665	0.5
24^3	0.3667	0.7
30^3	0.3669	0.7
48^3	0.3670	0.5
64^3	0.36705	0.5

"cylindrical" lattices to obtain the spectrum of the transfer matrix. These lattices were of size 120×20^2 for 18 values of β and with size 120×30^2 for 17 values of β, as summarized in Table II. Runs of as many as 2×10^6 sweeps made it possible to gain control of the correlated data and to obtain good estimates of the parameter errors.

A. Simulations on cubic lattices

In Fig. 2 is shown a histogram in the average energy for the 64^3 lattice near β_c. A clean separation of the phases is apparent. During this 250 000-sweep simulation two tunneling events were observed, in each case with the order parameter passing cleanly from one peak to the other in a single update step. The importance of finite-size scaling for determining the order of a phase transition has been repeatedly emphasized [6, 7]. Although these references already provide excellent confirmation of the first-order character of the phase transition, our high statistics results make an even stronger case. Nevertheless, we present the finite-size scaling results for the sake of completeness. The fourth-order cumulant [11],

$$V_L(\beta, V) = 1 - \frac{\langle E^4 \rangle}{3 \langle E^2 \rangle^2}, \tag{28}$$

TABLE II. Data sample for cylindrical lattices. (10^6 sweeps.)

β	120×20^2	120×30^2
0.3650	1.0	1.0
0.3655	—	1.0
0.3660	1.0	1.0
0.3665	1.0	1.0
0.3668	2.0	1.0
0.3669	2.0	2.0
0.36695	2.0	2.0
0.3670	2.0	2.0
0.36705	2.0	2.0
0.3671	2.0	2.0
0.36715	2.0	2.0
0.3672	3.0	2.0
0.36725	2.0	2.0
0.3673	1.0	1.0
0.3674	1.0	1.0
0.3675	1.0	1.0
0.3678	1.0	—
0.3680	1.0	1.0
0.3685	1.0	—

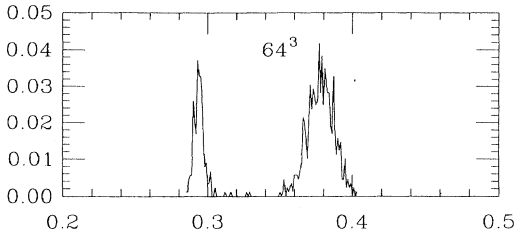

FIG. 2. Histogram in the average energy at $\beta = 0.36705$ (near the critical value) on a 64^3 lattice, showing cleanly separated coexisting phases.

is minimum near the crossover β_c. At a continuous phase transition, the minimum value $V_L(\beta_c, V)$ tends to $\frac{2}{3}$ in the infinite volume limit. At a first-order phase transition, however, the limit is not so constrained, but obeys a scaling law,

$$V_L(V)_{\min} \to 1 - \frac{(E_+^2 + E_-^2)^2}{12(E_+E_-)^2} + O(1/V), \tag{29}$$

where E_+ and E_- are the most probable energies in the two coexisting phases.

The minimum value of the cumulant was found by combining measurements at a range of β values near β_c, using a Ferrenberg-Swendson "scanning" or "histogram" technique [12]. The resulting minimum values are plotted in Fig. 3. A linear fit yields the asymptotic value 0.647(3), clearly distinct from $\frac{2}{3}$.

We turn now to the specific heat. At finite volume the specific heat C_v peaks at the crossover. The maximum value $C_{v,\max}$ increases with increasing volume. If the phase transition is first order, the peak scales as

$$C_{v,\max} = a + bV. \tag{30}$$

The maximum is again determined using the Ferrenberg-Swendson technique. These values are plotted in Fig. 4. A linear increase is apparent.

A value of β_c can be fixed, either from the peak in

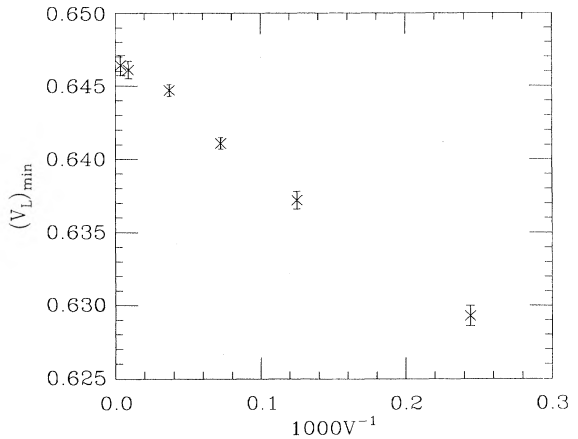

FIG. 3. Finite-size scaling of the minimum in the fourth-order cumulant.

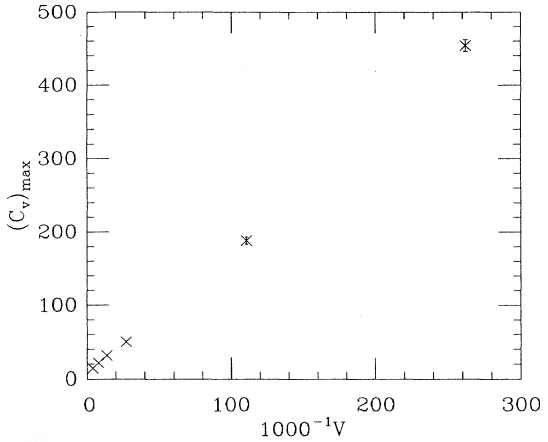

FIG. 4. Finite-size scaling of the peak in the specific heat.

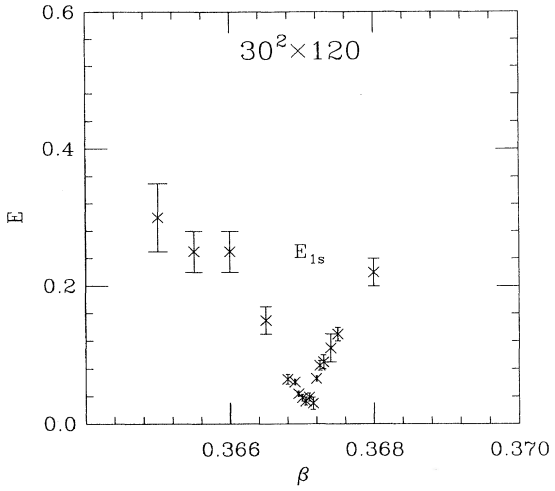

FIG. 6. The same, but for the $30^2 \times 120$ lattice.

the specific heat, or from the minimum of the cumulant V_L. The two values do not necessarily agree at finite volume, but should agree in the infinite volume limit. In the infinite volume limit we find $\beta_{c,\infty} = 0.36704(2)$ in agreement with Gavai, Karsch, and Petersson [6].

B. Simulations on cylindrical lattices

Measurements on the asymmetrical lattices were taken every 250 SW sweeps. Observables recorded were these: the spin averages $s(z)$ as a function of z [Eq. (18)], the average energy

$$E = \beta \sum_{(i\mu)} \mathrm{Re}\, s_i^* s_{i+\mu}/V, \tag{31}$$

and the number of clusters N_c. Subsequent analysis produced the symmetric and mixed operator correlations and spectrum, the mean spins, and the projected-spin order parameter

$$s_{\mathrm{proj}} = \max \mathrm{Re}(\bar{s}, e^{2\pi i/3}\bar{s}, e^{-2\pi i/3}\bar{s}), \tag{32}$$

where $\bar{s} = \sum s_i/V$. Also constructed were interface statistics. They are described below. For observables not discussed here, see Ref. [8].

(a) Spectrum of the transfer matrix. Correlations in the operators $|s(z)|^2$ and $s(z)$ were measured and fit to the formulas (27) for both transverse sizes 20^2 and 30^2. As usual, fluctuations in the measurements were strongly correlated in z, so it was necessary to determine these correlations and incorporate them in the χ^2 analysis. Because of the large size of the data sample, it was possible to use all principal factors in the analysis of covariance. The spectrum was determined from a global fit to the data. The fitting range began at a minimum distance z_{min} and extended to the full length of the lattice.

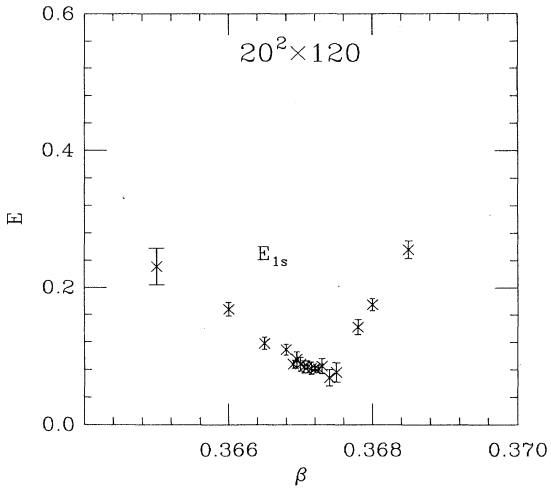

FIG. 5. Energy level E_{1s} of symmetry S for the $20^2 \times 120$ lattice, as a function of β.

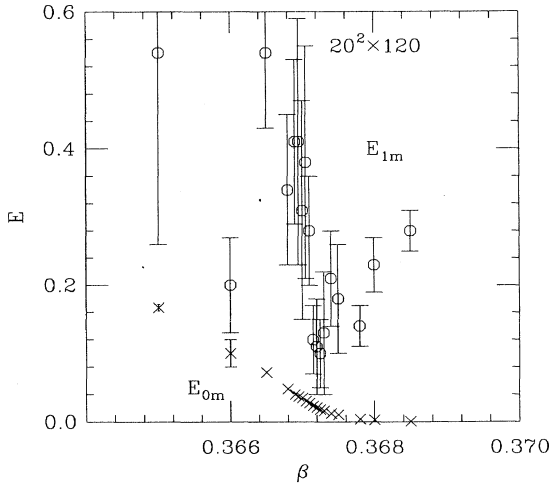

FIG. 7. Energy levels E_{0m} and E_{1m} of symmetry M for the $20^2 \times 120$ lattice, as a function of β.

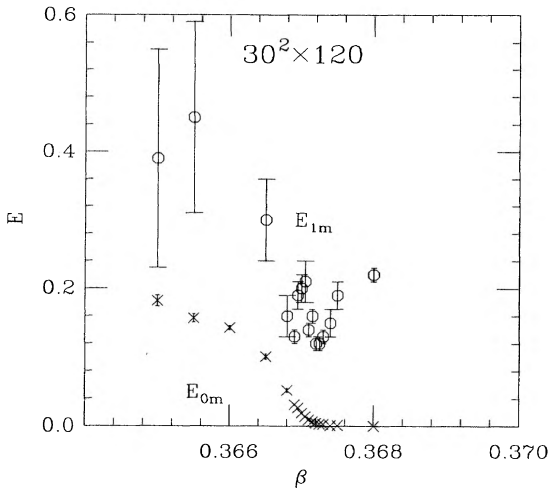

FIG. 8. The same, but for the $30^2 \times 120$ lattice.

The minimum distance was varied until a semblance of a plateau in the spectrum was reached, within the determined statistical errors. The values quoted are based on the minimum distance that gave the highest confidence level for the fit. The minimum distance thus determined varied smoothly from 2 for the mixed operator at the smallest β where the correlation length is shortest to 8 at the largest β where the correlation length is longest. For the symmetric operator $z_{\min}$ was 5 for the smallest and largest β's, ranging gradually to 15–20 for the intermediate values where the correlation length is longest. The resulting spectrum is summarized in Figs. 5–8 and in Tables III and IV. There is obviously a strong resemblance with features of the simple model of Sec. II B. From Figs. 7 and 8, we see that the correlation length tends to infinity as β increases above β_c, just as with lattices of similar geometry in SU(3) Yang-Mills theory [4]. As we have seen in the simple model, this feature is an expected consequence of finite volume tunneling between the degenerate ordered phases.

(b) Tunneling statistics. In Fig. 9 we plot the slice spin averages $s(z)$ for a representative configuration at $\beta > \beta_c$, showing tunneling between the ordered phases. We devised two statistics: $N_{\rm DO}$, to give a measure of the number of phase boundaries between the disordered and one of the ordered domains, and a statistic $N_{\rm OO}$, for phase boundaries between two ordered domains. A portion of the lattice was considered to be in the disordered phase on the plane z, if $|s(z)| < 0.23$ for at least three consecutive values of z. If $|s(z)| > 0.23$ for at least three consecutive values of z, the lattice plane was considered to be in one of the three ordered phases, according to the value of $\arg s(z)$. The value 0.23 was chosen to correspond to the minimum of the histogram of occurrences of values of $|s|$ at the crossover, and so corresponds to a value intermediate between the disordered and ordered phases. The requirement of three consecutive planes was adopted to permit occasional excursions from the ideal value of 0.23 within a single phase. We encountered no configurations that did not have at least three consecutive planes. Indeed the phase coherence was extremely high with many lattices consisting of a single phase.

Obviously our classification criteria are arbitrary. Our approach differs from that of Karsch and Patkós [13] who classified all boundaries as type OO for $\beta > \beta_c$. The ambiguity all methods must deal with is distinguishing a broad interface between two ordered phases from a transition to an intermediate disordered phase. Any definition must recognize, however, that in perturbation theory, finite volume mixing necessarily produces a disordered phase intermediate for β slightly above β_c.

Shown in Figs. 10–12 are results for the measure of the mean numbers $N_{\rm OO}$ and $N_{\rm DO}$. It is apparent that with

TABLE III. Effective masses and couplings for the 120×20^2 lattice.

β	A_1	A_2	E_{1s}	C_1	E_{0m}	C_2	E_{1m}
0.3650	2.38(1)	0.5(1)	0.231(27)	2.9(1)	0.167(5)	0.18(11)	0.54(28)
0.3660	3.20(3)	0.94(7)	0.168(10)	3.3(9)	0.10(2)	1.0(9)	0.20(7)
0.3665	4.36(4)	1.6(2)	0.118(9)	5.8(1)	0.072(1)	0.31(4)	0.54(11)
0.3668	6.11(6)	2.6(3)	0.109(8)	8.0(1)	0.048(1)	0.30(5)	0.34(11)
0.3669	7.17(7)	2.5(2)	0.088(6)	9.3(1)	0.0397(6)	0.34(9)	0.41(12)
0.36695	7.8(1)	2.9(4)	0.095(11)	10.1(2)	0.037(1)	0.34(1)	0.41(18)
0.3670	8.51(8)	2.7(4)	0.088(10)	10.8(1)	0.0346(6)	0.24(6)	0.31(16)
0.36705	9.59(9)	2.8(4)	0.084(9)	11.8(1)	0.0302(4)	0.26(8)	0.38(17)
0.3671	10.5(1)	3.0(4)	0.084(9)	12.4(1)	0.0272(4)	0.35(5)	0.28(8)
0.36715	11.8(1)	2.8(4)	0.082(9)	13.2(3)	0.0233(6)	0.6(3)	0.12(5)
0.3672	13.2(1)	2.8(1)	0.082(3)	14.1(4)	0.0207(6)	0.5(3)	0.11(7)
0.36725	14.4(1)	2.6(2)	0.081(5)	14.5(6)	0.0180(7)	0.8(4)	0.10(5)
0.3673	15.8(2)	2.8(4)	0.085(11)	15.4(4)	0.0159(7)	0.8(2)	0.14(9)
0.3674	18.6(2)	1.8(2)	0.068(12)	16.2(3)	0.0122(5)	1.8(8)	0.21(7)
0.3675	20.7(2)	1.5(3)	0.076(14)	16.9(3)	0.0102(5)	0.9(3)	0.18(8)
0.3678	25.5(1)	1.3(1)	0.142(11)	15.6(5)	0.0039(6)	1.3(1)	0.14(3)
0.3680	27.2(1)	1.12(5)	0.175(9)	15.9(4)	0.0029(4)	1.2(2)	0.23(4)
0.3685	30.4(1)	1.03(6)	0.256(13)	15.7(3)	0.0007(3)	1.2(1)	0.28(3)

TABLE IV. Effective masses and couplings for the 120×30^2 lattice.

β	A_1	A_2	E_{1s}	C_1	E_{0m}	C_2	E_{1m}
0.3650	1.02(1)	0.2(1)	0.30(5)	1.2(1)	0.182(8)	0.1(1)	0.39(16)
0.3655	1.11(1)	0.23(6)	0.25(3)	1.29(8)	0.157(6)	0.15(7)	0.45(14)
0.3660	1.23(1)	0.38(8)	0.25(3)	1.56(2)	0.143(3)	—	—
0.3665	1.48(1)	0.44(9)	0.15(2)	1.74(9)	0.101(4)	0.24(9)	0.30(6)
0.3668	2.03(3)	0.74(6)	0.065(7)	2.3(2)	0.052(3)	0.59(18)	0.16(3)
0.3669	3.21(6)	1.28(5)	0.061(4)	3.7(1)	0.031(1)	0.72(12)	0.13(1)
0.36695	4.09(9)	1.61(4)	0.044(4)	5.2(1)	0.0262(6)	0.39(4)	0.19(2)
0.3670	6.3(2)	2.02(7)	0.038(5)	7.3(1)	0.0185(3)	0.41(3)	0.20(2)
0.36705	9.9(3)	2.1(1)	0.033(6)	9.9(1)	0.0133(2)	0.38(3)	0.21(3)
0.3671	14.4(2)	1.6(1)	0.039(6)	11.8(1)	0.0092(2)	0.55(4)	0.14(1)
0.36715	17.4(3)	1.3(2)	0.030(9)	12.6(1)	0.0064(2)	0.65(3)	0.16(1)
0.3672	19.6(1)	0.98(3)	0.066(4)	12.5(2)	0.0044(2)	0.75(4)	0.12(1)
0.36725	20.9(1)	0.85(8)	0.085(7)	12.2(2)	0.0028(2)	0.86(3)	0.12(1)
0.3673	21.6(1)	0.7(1)	0.09(1)	12.6(2)	0.0027(3)	0.73(4)	0.13(1)
0.3674	23.1(1)	0.5(2)	0.11(2)	12.3(3)	0.0011(4)	0.69(4)	0.15(2)
0.3675	24.1(1)	0.5(1)	0.13(1)	12.7(2)	0.0010(3)	0.8(1)	0.19(2)
0.3680	27.8(1)	0.50(7)	0.22(2)	14.0(3)	0.0001(3)	0.50(5)	0.22(1)

our definitions of these boundaries, a transition between two ordered phases is unlikely to take place directly, but proceeds through what we identify as a disordered phase intermediate. (Figure 10 shows the number of OO phase boundaries for the 120×20^2 lattices. The corresponding number for 120×30^2 is negligible.) This "complete wetting" effect was reported previously in SU(3) gauge theory [14] and the Potts model [13].

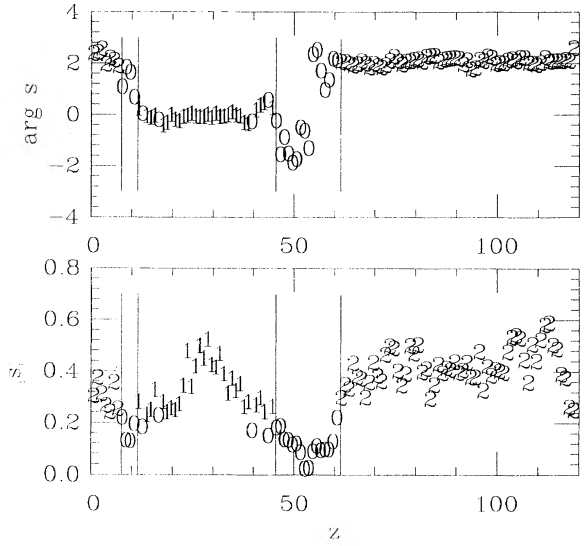

FIG. 9. Plot of the complex modulus and argument of the spin vector $s(z)$ vs z (averaged over the transverse plane) for a typical configuration selected from the data sample at $\beta = 0.3672$ (near the phase transition) on a $20^2 \times 120$ lattice. The plot symbol indicates the phase to which the lattice plane is assigned, based on modulus and argument. The vertical bars indicate an assigned phase boundary, based on our arbitrary rule that at least three consecutive planes must be classified in that phase. The horizontal line in the modulus plot indicates our division between ordered and disordered phases. Two ordered-ordered phase boundaries appear in this configuration, each with a disordered phase intermediate.

As a test of the sensitivity of the phase boundary statistics to our definition of the phases, we analyzed the results for our $20^3 \times 120$ lattices at $\beta = 0.3672$ and at $\beta = 0.3675$ for a variety of choices of the required number of consecutive planes with $s(z)$ in the same phase. Results are tabulated in the first four columns of Table V. As expected, the number N_{DO} decreases as we require more consecutive planes before deciding that a transition to a new phase has taken place. However, the number N_{OO} of direct ordered-ordered phase boundaries is still extremely small. The fact that N_{DO} decreases more dramatically than the increase in N_{OO} indicates that the small pockets of low $|s(z)|$ are often sandwiched between regions with larger $|s(z)|$, but with the same orientation. Thus these results support our assumption that these

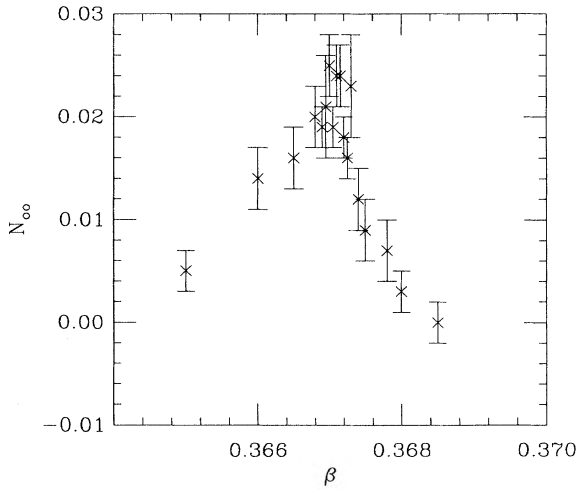

FIG. 10. Average number of phase boundaries separating ordered symmetry phases for 120×20^2.

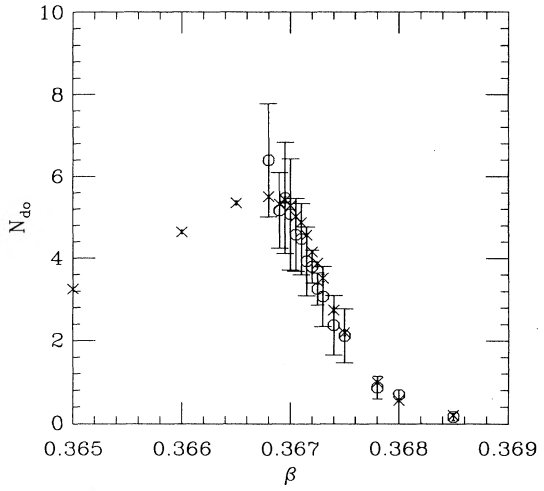

FIG. 11. Average number of phase boundaries separating a disordered phase from an ordered phase for 120×20^2. Crosses are measured directly. Octagons are calculated from the spectrum in the four-component model.

small pockets are more properly associated with the ordered phase that surrounds it, and should not be counted as a complete phase boundary.

Interpreting these results in terms of the model of Sec. II B, we find that $\epsilon \ll \lambda$. Thus the approximation, Eqs. (15)–(17), applies. Inverting these expressions, the parameters Δ and λ of the simple model can then be derived directly from the observed spectrum through

$$\Delta = E_{1s} - 2E_{0m}, \tag{33}$$

$$\lambda = \sqrt{E_{0m}(E_{1s} - E_{0m})/3}. \tag{34}$$

Let us compare the Potts phase boundary statistics with what is expected in the four-component model. We do so in the complete wetting approximation that $\epsilon = 0$. With $\epsilon = 0$, necessarily $N_{\mathrm{DD}} = 0$, and a simple computation gives N_{DO}. Since λ in the four-component Hamiltonian mixes the disordered and ordered states, we can introduce a chemical potential for DO boundaries by replacing λ with λe^{μ}. Thus the number of DO boundaries is just

$$\langle N_{\mathrm{DO}} \rangle = \lambda \frac{\partial}{\partial \lambda} \ln Z, \tag{35}$$

but from Eqs. (2), (6), and (15) we have $\ln Z \approx -LE_{0s}(\lambda)$, so

$$\langle N_{\mathrm{DO}} \rangle \approx 6L\lambda^2/\sqrt{\Delta^2 + 12\lambda^2}. \tag{36}$$

Using this expression at $\beta = 0.3672$ for the $20^2 \times 120$ lattice we calculate $\langle N_{\mathrm{DO}} \rangle = 3.7(4)$, and at $\beta = 0.3675$, 2.1(7). The rather large uncertainty is due to the uncertainties in the spectrum. Comparing these values with those tabulated in Table V, we see that the values agree if the consecutive run criterion is 3 or 4, thereby justifying our procedure for counting phase boundaries.

In the four-component model it is possible to create domains of width one slice. Clearly, if we impose the same consecutive-run criterion on the four-component model, we overlook genuine boundaries and bias the statistics. We analyzed this effect using a simple numerical simulation of the corresponding one-dimensional statistical system. Results for the two cases of interest are tabulated in the last two columns of Table V for comparison. The largest uncertainty in these results arises from the uncertainty in the determination of the spectral values E_{1s} and E_{0m}, which, through Eq. (34), determine the parameters of the four-component model. To make a quick estimate of the error propagation, we use the exact result for a run length of one above (36). That result is quoted in the table. We see that going from a run of one to a run of three reduces $\langle N_{\mathrm{DO}} \rangle$ by about 0.5 at the lower value of β and by about 0.3 at the upper value. These systematic errors are comparable or smaller than the uncertainties arising from the determination of the spectrum, so we ignore them. (We emphasize that we should not compare the tabulated values for the two model calculations line by line, since in our interpretation the variation in the Potts model value is attributed to a possible nontrivial interface width, the counting of false boundaries, and the omission of genuine boundaries, whereas the variation in the four-component model value is due solely to the omission of genuine boundaries.)

Returning to Eq. (36), we compute the predicted value of N_{DO} in the four-component model for runs of length three for all $\beta > \beta_c$ for both $20^2 \times 120$ and $30^2 \times 120$ lattices. Results are plotted together with the observed number in Figs. 11 and 12. With our criteria for identifying a phase boundary the agreement is quite satisfactory.

(c) Surface tension. The surface tension between two ordered phases can be estimated in perturbation theory through

$$\lambda = \delta e^{-\beta \alpha_{\mathrm{OD}} A}. \tag{37}$$

A formula of this type was conjectured by Brezin and Zinn-Justin [16]. The quantity on the left is the transition probability between two ordered phases via a disordered phase intermediate in second-order perturbation

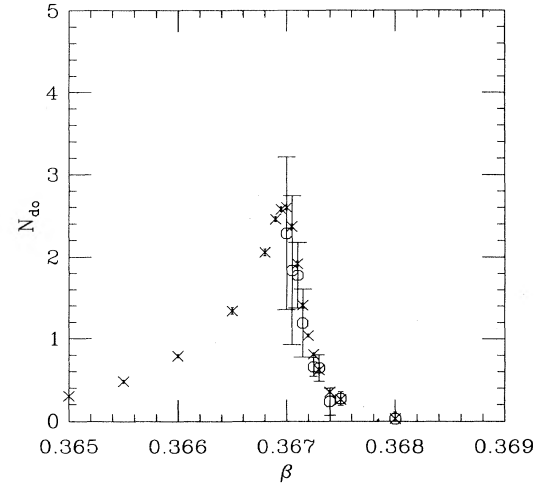

FIG. 12. Same as Fig. 11, but for 120×30^3.

TABLE V. Phase boundary statistics as a function of run count for the 120×20^2 lattice.

		Potts model		Four-component model	
β	run	N_{DO}	N_{OO}	N_{DO}	N_{OO}
0.3672	1	10.94(7)	0.175(7)	3.8(4)	0.00
0.3672	2	5.67(4)	0.022(2)	3.5(4)	0.02
0.3672	3	4.16(3)	0.018(2)	3.3(4)	0.04
0.3672	4	3.44(3)	0.032(2)	3.0(4)	0.06
0.3672	5	2.98(2)	0.050(3)	2.8(4)	0.07
0.3672	10	1.74(2)	0.154(6)	2.0(4)	0.09
0.3675	1	6.06(10)	0.108(9)	2.2(7)	0.00
0.3675	2	3.03(6)	0.014(3)	2.0(7)	0.01
0.3675	3	2.19(5)	0.012(2)	1.8(7)	0.02
0.3675	4	1.71(4)	0.013(2)	1.7(7)	0.02
0.3675	5	1.41(4)	0.027(4)	1.6(7)	0.02
0.3675	10	0.73(2)	0.078(7)	1.0(7)	0.02

theory, based on the four-component Hamiltonian, and the quantity on the right is the Boltzmann weight for the interface. The prefactor δ takes account of capillary waves on the interface. It is independent of the transverse size of the lattice [16]. Following Grossman *et al.* [17], we treat δ as an unknown constant and determine α_{OD} by comparing results from the two lattice sizes. Thus estimated, it is plotted in Fig. 13.

IV. SUMMARY AND DISCUSSION

Our high statistics study of the three-state three-dimensional Potts model using the Swendson-Wang updating scheme once again confirms the first-order character of the phase transition. At volumes as large as 64^3 there is a clear separation of coexisting phases.

Exploiting an S_3 symmetry in lattices with one long dimension, we have obtained the lowest spectral levels of the transfer matrix in this model and find a strong resemblance with the spectrum of a simple four-component model, featuring a first-order phase transition. This analysis provides a clear explanation of the mechanism that gives rise to an infinite correlation length in the low-temperature phase.

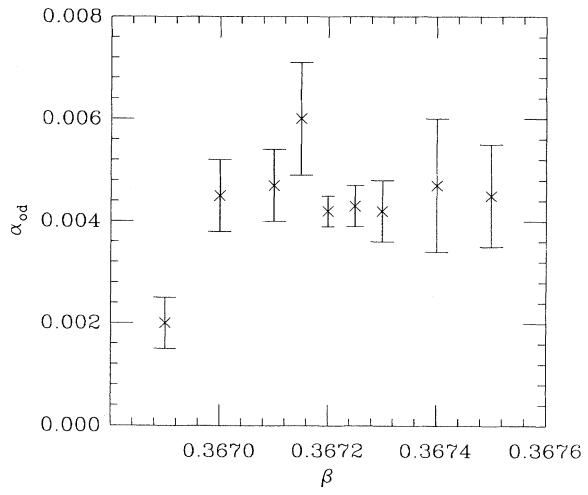

FIG. 13. Ordered-disordered interface surface tension determined by spectral methods in the four-component model.

The statistics of phase boundaries at low temperature are consistent with a perturbative treatment of tunneling in the four-component model. We find that ordered-ordered phase boundaries involve an intermediate disordered phase consistent with complete wetting. We obtained the ordered-disordered surface tension from the spectrum.

One important goal of finite-size spectral analysis is to remove tunneling-related finite-size effects from the spectrum, with the hope of extracting the infinite volume values of the excitation spectrum. Would this be feasible using our methods? Unfortunately, to remove significant finite-size effects apparently requires introducing more parameters into the four-component model and into our fitting functions than data of the quality of ours warrants. The four-component model would have to be augmented by at least four more components. Thus we must rely upon alternate, empirical methods. For example, Fukugita and Okawa [7] calculate in a cubic volume. In the vicinity of the phase transition, they classify configurations into two groups: disordered and ordered, according to the value of the global-order parameter. They then measure "pure-phase" correlation lengths in each subset. For small volumes there is a region of overlap in which this classification risks misidentification of the phase. The contamination of incorrectly classified configurations decreases as the volume is increased and the overlap decreases. Thus one may hope for an empirically determined extrapolation to the infinite volume limit.

ACKNOWLEDGMENTS

Helpful conversations with Bernard Grossmann, Morten Laursen, and Thomas Trappenburg are gratefully acknowledged. We are indebted to them for supplying us with an advance copy of their paper. Computations were carried out in the initial portion of this work on an IBM 3090/600S at the Utah Supercomputing Institute and on a Cray Y/MP at the San Diego Supercomputer Center, and in later portion, on IBM RS 6000/320 workstations in the Department of Physics, University of Utah.

[1] B. Svetitsky and L.G. Yaffe, Phys. Rev. D **26**, 963 (1982); Nucl. Phys. **B210**, 423 (1982); J. Polónyi and K. Szlachányi, Phys. Lett. **100B**, 395 (1982); T.A. DeGrand and C.E. DeTar, Nucl. Phys. **B225** [FS9], 590 (1983); F. Green and F. Karsch, *ibid.* **B238**, 297 (1984); M. Okawa, Phys. Rev. Lett. **60**, 1805 (1988).

[2] J.P. Straley and M.E. Fisher, J. Phys. A **6**, 1310 (1973); L. Susskind, Phys. Rev. D **20**, 2610 (1979); S.J. Knak Jensen and O.G. Mouritsen, Phys. Rev. Lett. **43**, 1736 (1979); F.Y. Wu, Rev. Mod. Phys. **54**, 235 (1982).

[3] A. Ukawa, in *Lattice '89*, Proceedings of the International Symposium, Capri, Italy, 1989, edited by R. Petronzio *et al.* [Nucl. Phys. B (Proc. Suppl.) **17**, 118 (1990)].

[4] APE Collaboration, P. Bacilieri *et al.*, Phys. Rev. Lett. **61**, 1545 (1988); Nucl. Phys. **B318**, 553 (1989).

[5] F.R. Brown, N.H. Christ, Y. Deng, M. Gao, and T.J. Woch, Phys. Rev. Lett. **61**, 2058 (1988).

[6] R.V. Gavai, F. Karsch, and B. Petersson, Nucl. Phys. **B322**, 738 (1989); R.V. Gavai, S. Gupta, A. Irbäck, F. Karsch, and B. Petersson, *ibid.* **B329**, 263 (1990).

[7] M. Fukugita, M. Okawa, and A. Ukawa, Phys. Rev. Lett. **63**, 1768 (1989); Nucl. Phys. **B337**, 181 (1990); M. Fukugita and M. Okawa, Phys. Rev. Lett. **63**, 13 (1989).

[8] Jing-Dong Wang, Ph.D. thesis, University of Utah, 1992.

[9] K. Jansen, J. Jersak, I. Montvay, G. Münster, T. Trappenberg, and U. Wolff, Phys. Lett. B **213**, 203 (1988).

[10] R.H. Swendson and J.-S. Wang, Phys. Rev. Lett. **58**, 86 (1987).

[11] M.S. Challa, D.P. Landau, and K. Binder, Phys. Rev. B **34**, 1841 (1986).

[12] A.M. Ferrenberg and R.H. Swendson, Phys. Rev. Lett. **61**, 2643 (1988).

[13] F. Karsch and A. Patkós, Nucl. Phys. **B350**, 563 (1991).

[14] K. Kajantie, L. Kärkkäinen, and K. Rummukainen, Nucl. Phys. **B357**, 693 (1991).

[15] T. Trappenberg and U.J. Wiese, Nucl. Phys. **B372**, 703 (1992).

[16] E. Brezin and J. Zinn-Justin, Nucl. Phys. **B257**, 867 (1985); V. Privman and M.E. Fisher, J. Stat. Phys. **33**, 385 (1983).

[17] B. Grossmann, M.L. Laursen, T. Trappenberg, and U.-J. Wiese, HLRZ Jülich Report No. 92-47, 1992 (unpublished).